Microring resonator photodetector for enhancement in *L*-band performance

Junfeng Song,[1,2*] Andy Lim Eu-Jin,[1] Xianshu Luo,[1] Ying Huang,[1] Xiaoguang Tu,[1] Lianxi Jia,[1] Qing Fang,[1] Tsung-Yang Liow,[1] Mingbin Yu[1] and Guo-Qiang Lo[1]

[1]*Institute of Microelectronics, A*STAR (Agency for Science, Technology and Research), 11 Science Park Road, Science Park II, Singapore 117685 Singapore*

[2]*State Key Laboratory on Integrated opto-electronics, College of Electronic Science and Engineering, Jilin University, Changchun, People's Republic of China, 130012 China*

songjf@ime.a-star.edu.sg

Abstract: We proposed a microring resonator (MRR) enhanced photodetector (PD) structure. Resonance wavelength enhanced by the MRR amplifies the PD response. At *L*-band wavelengths, responsivity was doubled for an ultra-short germanium PD of 4 μm employing the MRR structure. Data rates of up to 40 Gb/s were also demonstrated at 1600 nm.

OCIS codes: (130.0250) Optoelectronics; (130.3120) Integrated optics devices; (130.7408) Wavelength filtering devices; (040.5160) Photodetectors; (250.5300) Photonic integrated circuits; (250.0040) Detectors; (250.3140) Integrated optoelectronic circuits; (280.6780) Temperature;

References and links

1. L. Pavesi and G. Guillot, Optical interconnects: the Silicon approach, (Springer Verlag, 2006).
2. A. Barkai, Y. Chetrit, O. Cohen, R. Cohen, N. Elek, E. Ginsburg, S. Litski, A. Michaeli, O. Raday, D. Rubin, G. Sarid, N. Izhaky, M. Morse, O. Dosunmu, A. Liu, L. Liao, H. Rong, Y.- Kuo, S. Xu, D. Alduino, J. Tseng, H.-F. Liu, and M. Paniccia, "Integrated silicon photonics for optical networks," J. Opt. Netw. **6**(1), 25–47 (2007).
3. Y. Vlasov, "Silicon photonics for next generation computing systems," in Proceedings of IEEE Conference on European Conference of Optical Communications (Brussels, Belgium, 2008).
4. D. Miller, "Device requirements for optical interconnects to silicon chips," Proc. IEEE **97**(7), 1166–1185 (2009).
5. A. E.-J. Lim, J. Song, Q. Fang, C. Li, X. Tu, N. Duan, K. K. Chen, R. P.-C. Tern, and T.-Y. Liow, "Review of Silicon Photonics Foundry Efforts," IEEE J. Sel. Top. Quantum Electron. **20**(4), 8300112 (2014).
6. Q. Fang, J. F. Song, T. Y. Liow, H. Cai, M. B. Yu, G. Q. Lo, and D. L. Kwong, "Ultralow power silicon photonics thermo-optic switch with suspended phase arms," IEEE Photon. Technol. Lett. **23**(8), 525–527 (2011).
7. T.-Y. Liow, J. Song, X. Tu, A.-J. Lim, Q. Fang, N. Duan, M. Yu, and G.-Q. Lo, "Silicon Optical Interconnect Device Technologies for 40 Gb/s and Beyond," IEEE J. Sel. Top. Quantum Electron. **19**(2), 8200312 (2013).
8. A. E.-J. Lim, T.-Y. Liow, F. Qing, N. Duan, L. Ding, M. Yu, G.-Q. Lo, and D.-L. Kwong, "Novel Evanescent-Coupled Germanium Electro-Absorption Modulator Featuring Monolithic Integration with Germanium p-i-n Photodetector," Opt. Express **19**(6), 5040–5046 (2011).
9. X. Tu, T.-Y. Liow, J. Song, X. Luo, Q. Fang, M. Yu, and G.-Q. Lo, "50-Gb/s silicon optical modulator with traveling-wave electrodes," Opt. Express **21**(10), 12776–12782 (2013).
10. D. J. Thomson, F. Y. Gardes, J.-M. Fedeli, S. Zlatanovic, Y. Hu, B. P. P. Kuo, E. Myslivets, N. Alic, S. Radic, G. Z. Mashanovich, and G. T. Reed, "50-Gb/s silicon optical modulator," IEEE Photon. Technol. Lett. **24**(4), 234–236 (2012).
11. P. Dong, S. Liao, D. Feng, H. Liang, D. Zheng, R. Shafiiha, C. C. Kung, W. Qian, G. Li, X. Zheng, A. V. Krishnamoorthy, and M. Asghari, "Low Vpp, ultralow-energy, compact, high-speed silicon electro-optic modulator," Opt. Express **17**(25), 22484–22490 (2009).
12. H. Byun, J. Bok, K. Cho, K. Cho, H. Choi, J. Choi, S. Choi, S. Han, S. Hong, S. Hyun, T. J. Jeong, H.-C. Ji, I.-S. Joe, B. Kim, D. Kim, J. Kim, J.-K. Kim, K. Kim, S.-G. Kim, D. Kong, B. Kuh, H. Kwon, B. Lee, H. Lee, K. Lee, S. Lee, K. Na, J. Nam, A. Nejadmalayeri, Y. Park, S. Parmar, J. Pyo, D. Shin, J. Shin, Y.- Shin, S.-D. Suh, H. Yoon, Y. Park, J. Choi, K.-H. Ha, and G. Jeong, "Bulk-Si photonics technology for DRAM interface," Photonics Research **2**(3), A25–A33 (2014).
13. J. Song, X. Luo, X. Tu, L. Jia, Q. Fang, T.-Y. Liow, M. Yu, and G.-Q. Lo, "Three-dimensional (3D) monolithically integrated photodetector and WDM receiver based on bulk silicon wafer," Opt. Express **22**(16), 19546–19554 (2014).
14. L. Vivien, J. Osmond, J. M. Fédéli, D. Marris-Morini, P. Crozat, J. F. Damlencourt, E. Cassan, Y. Lecunff, and S. Laval, "42 GHz p.i.n Germanium photodetector integrated in a silicon-on-insulator waveguide," Opt. Express **17**(8), 6252–6257 (2009).
15. Q. Fang, L. Jia, J. Song, A. E. Lim, X. Tu, X. Luo, M. Yu, and G. Lo, "Demonstration of a vertical pin Ge-on-Si photo-detector on a wet-etched Si recess," Opt. Express **21**(20), 23325–23330 (2013).

#221622 - $15.00 USD Received 25 Aug 2014; revised 18 Sep 2014; accepted 19 Sep 2014; published 23 Oct 2014

16. T. Y. Liow, K. W. Ang, Q. Fang, J. F. Song, Y. Z. Xiong, M. B. Yu, G. Q. Lo, and D. L. Kwong, "Silicon modulators and germanium photodetectors on SOI: Monolithic integration, compatibility, and performance optimization," IEEE J. Sel. Top. Quantum Electron. **16**(1), 307–315 (2010).
17. O. I. Dosunmu, D. D. Cannon, M. K. Emsley, L. C. Kimerling, and M. Unlu, "High-speed resonant cavity enhanced Ge photodetectors on reflecting Si substrates for 1550-nm operation," IEEE Photon. Technol. Lett. **17**(1), 175–177 (2005).
18. M. Casalino, L. Sirleto, L. Moretti, and I. Rendina, "A silicon compatible resonant cavity enhanced photodetector working at 1.55 μm," Semicond. Sci. Technol. **23**(7), 075001 (2008).
19. K. C. Balram, R. M. Audet, and D. A. Miller, "Nanoscale resonant-cavity-enhanced germanium photodetectors with lithographically defined spectral response for improved performance at telecommunications wavelengths," Opt. Express **21**(8), 10228–10233 (2013).
20. J. R. Jain, D.-S. Ly-Gagnon, K. C. Balram, J. S. White, M. L. Brongersma, D. A. Miller, and R. T. Howe, "Tensile-strained germanium-on-insulator substrate fabrication for silicon-compatible optoelectronics," Opt. Mater. Express **1**(6), 1121–1126 (2011).
21. J. F. Song, S. H. Tao, Q. Fang, T. Y. Liow, M. B. Yu, G. Q. Lo, and D. L. Kwong, "Thermo-optical enhanced silicon wire interleavers," IEEE Photon. Technol. Lett. **20**(24), 2165–2167 (2008).
22. J. Song, H. Zhao, Q. Fang, S. H. Tao, T. Y. Liow, M. B. Yu, G. Q. Lo, and D. L. Kwong, "Effective thermo-optical enhanced cross-ring resonator MZI interleavers on SOI," Opt. Express **16**(26), 21476–21482 (2008).
23. G. Ghione, *Semiconductor Devices for High-Speed Optoelectronics* (Cambridge University Press, 2009).
24. J. Song, X. Luo, X. Tu, M. K. Park, J. S. Kee, H. Zhang, M. Yu, G. Q. Lo, and D. L. Kwong, "Electrical tracing-assisted dual-microring label-free optical bio/chemical sensors," Opt. Express **20**(4), 4189–4197 (2012).
25. J. Song, X. Luo, J. S. Kee, K. Han, C. Li, M. K. Park, X. Tu, H. Zhang, Q. Fang, L. Jia, Y. J. Yoon, T. Y. Liow, M. Yu, and G. Q. Lo, "Silicon-based optoelectronic integrated circuit for label-free bio/chemical sensor," Opt. Express **21**(15), 17931–17940 (2013).
26. J. F. Song, X. S. Luo, J. S. Kee, Q. Liu, K. W. Kim, Y. Shin, M. K. Park, K. W. Ang, and G. Q. Lo, A Novel Optical Multiplexed, Label-Free Bio-Photonic-Sensor Realized on CMOS-Compatible Optoelectronic Integrated Circuit (OEIC) Platform," in Electron Devices Meeting (IEDM), 2013 IEEE International, pp. 381–384.

1. Introduction

In the past decade, silicon-on-insulator (SOI) based silicon photonics integrated devices and systems have received wide attention and seen rapid development [1–5]. These range from ultra-low power consumption optical switches [6,7] to high speed and efficient active devices [8–11], and bulk-Si based photonic technology platform [12,13]. The photodetector (PD) is a key component in various photonic applications, and state-of-the-art SOI based PD bandwidths are in excess of 20 GHz with ~1 A/W responsivity [5, 14–16]. At present, Germanium is the preferred choice for detection in the mid infra-red regime, in particular, telecommunication wavelengths of 1310 nm and 1550 nm. However, for wavelengths in the *L*-band (> 1580 nm), there is lower absorption due to a roll-off in the Ge absorption edge. To get higher responsivity, the length of the PD must be increased. Inevitably, this comes along with a trade-off in bandwidth reduction.

A cavity enhancement structure can be applied to overcome the reduction in frequency response [17,18]. In addition, tensile strain has also been used to enhance Ge absorption beyond its direct bandgap [19,20]. In this paper, we propose an alternative microring resonator (MRR) enhanced PD structure for compactness. This MRR structure enhances light detection in the *L*-band, while allowing a very short PD length to attain high device bandwidth. An integrated thermal heater was also included in the MRR to tune the oscillation wavelength. The modeling of MRR enhanced PD structure is described in this paper, together with characterization to verify this concept.

2. Modeling of MRR enhanced PD structure

2.1 Light intensity enhancement factor

A waveguide coupled PD and proposed MRR enhanced PD is illustrated in Fig. 1(a) and 1(b), respectively, for comparison. The waveguide coupled PD consists of a channel waveguide coupling light into a Ge-PD. The proposed MRR enhanced structure has a Ge-PD formed at the microring whereby interference effect allows the oscillation wavelength light to be enhanced by the MRR. The enhancement factor *M* can be used to describe the light intensity proportion between inside MRR and incident light, and it can be given in Eq. (1) as:

#221622 - $15.00 USD Received 25 Aug 2014; revised 18 Sep 2014; accepted 19 Sep 2014; published 23 Oct 2014

$$M = \frac{\kappa^2}{1 - 2t\gamma\cos(\theta) + t^2\gamma^2} \tag{1}$$

where t and κ are through- and cross- coupling coefficients, respectively, and should satisfy the relationship of $t^2 + \kappa^2 = 1$. γ is the amplitude loss factor of light per round in the MRR, and θ is phase shift of whole ring.

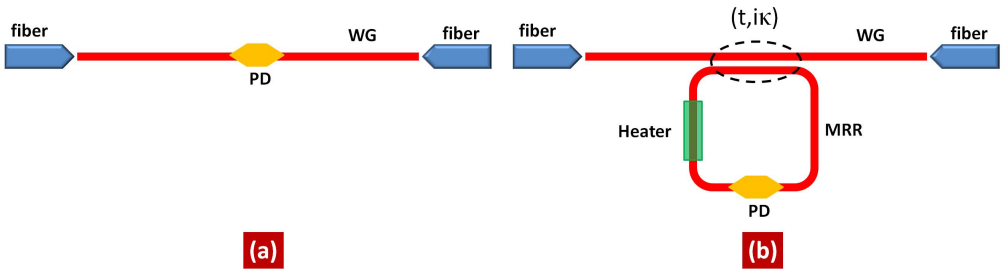

Fig. 1. Schematic illustrations for (a) the waveguide coupled photodetector, and (b) the proposed microring resonator (MRR) enhanced photodetector. The coupling region of microring and waveguide are denoted by dished ellipse. The coupling coefficients are t and κ respectively. The heater tuning region is denoted by a green color.

A lossless system has $\gamma = 1$, but in a practical system, γ is influenced by the waveguide loss γ_w, and the PD induced optical loss γ_{PD} by the relationship of $\gamma = \gamma_w\gamma_{PD}$. The waveguide loss γ_w is due to materials absorption and surface scattering, while γ_{PD} can be characterized by the Ge absorption and coupling loss between the waveguide and PD. To reduce PD loss, three measures were adopted. Firstly, a wet silicon etch was done to reduce the height difference between Ge-PD and Si waveguide which allowed butt-coupling between Si waveguide and Ge-PD. Secondly, a Ge taper was formed at both the input and output of the PD structure. And thirdly, a rib waveguide structure was used for the Ge-PD to reduce horizontal radiation loss. These will be elaborated further in Section 3.

The oscillation wavelength is given as $\theta = 2N\pi$, where N is an integer number. For a lossless system, the Eq. (1) can be simplified as Eq. (2) for the oscillation wavelength.

$$M_{os} = \frac{1+t}{1-t} \tag{2}$$

where M_{os} indicate the oscillation wavelength enhancement factor. From Eq. (2), we can see that M is determined by coupling coefficient t. When t gets closer to 1, M_{os} increases. If we take account of a lossy system, the Eq. (2) is rewritten as:

$$M_{os} = \frac{\kappa^2}{(1-t\gamma)^2} \tag{3}$$

Figure 2 shows the relationship of M_{os} with coupling coefficient t. The green color filled region is when the enhancement factor is bigger than 1. Unlike a lossless situation (indicated by red dished line), to get M_{os} larger than 1, t must be smaller than $2\gamma/(1 + \gamma^2)$. When t is equal to loss factor γ, the enhancement factor M_{os} is maximum at a value of $1/(1-\gamma^2)$. A lower loss and a higher coefficient t will increase the enhancement factor M_{os}.

#221622 - $15.00 USD Received 25 Aug 2014; revised 18 Sep 2014; accepted 19 Sep 2014; published 23 Oct 2014

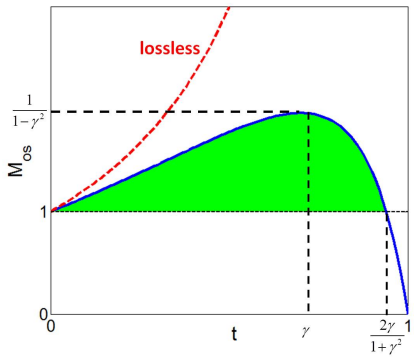

Fig. 2. Comparison of amplitude enhancement factor with or without loss. Red dished line demarks a lossless situation, while the blue solid line shows the lossy state. Green color filled region is enhancement factor larger than 1.

2.2 Bandwidth of MRR PD

The electric field E_r of MRR is related to the input electric field E_0 through Eq. (4):

$$E_r = E_0 \frac{i\kappa}{1 - t\gamma \exp(i\theta)} \tag{4}$$

For microwave modulated small signal situation, the incident light frequency is further expanded as shown in Eq. (5). Where t' is the time, υ is the light frequency, and υ_f is the microwave modulation frequency.

$$E = E_0 \sin(\pi \upsilon_f t') \exp(2\pi i \upsilon t') = \frac{E_0}{2i}\left\{\exp\left[2\pi i\left(\upsilon + \frac{\upsilon_f}{2}\right)t'\right] - \exp\left[2\pi i\left(\upsilon - \frac{\upsilon_f}{2}\right)t'\right]\right\} \tag{5}$$

Substituting Eq. (5) into Eq. (4), the light in MRR can be defined as Eq. (6):

$$\left|E_r\right|^2 = \left|E_{r+} + E_{r-}\right|^2 = \frac{1}{2}E_0^2\kappa^2 \frac{1 + \cos(2\pi\upsilon_f t' + \vartheta)}{(1 - t\gamma)^2 + 4t\gamma \sin^2\left(\frac{\pi\upsilon_f \tau}{2}\right)} \tag{6}$$

where $\tau = n_g L/c$ is the time the incident light completes a loop in the MRR, n_g is group index of waveguide, L is the perimeter of the microring and c is speed of light in vacuum. Therefore, the MRR enhanced PD response, $\Re(\upsilon_f)$ can be described as in Eq. (7) whereby the first term in right side of equation is the independent modulation frequency response, the second term is PD frequency response, and the third term is MRR induced frequency dependent response.

$$\left|\Re(\upsilon_f)\right|^2 = \left|\Re(0)\right|^2 \frac{1}{1 + \left(\frac{\upsilon_f}{\upsilon_{3dB,PD}}\right)^2} \frac{1}{1 + \frac{4t\gamma}{(1 - t\gamma)^2}\sin^2\left(\frac{\pi\upsilon_f \tau}{2}\right)} \tag{7}$$

where $\upsilon_{3dB,PD}$ is 3-dB bandwidth of the PD. If perimeter of MRR is small enough, it can be assumed $\upsilon_f \tau \ll 1$. In this case, Eq. (7) can be reduced to Eq. (8) to approximate the 3-dB bandwidth. When $t\gamma$ is small, the influence of MRR is small too. With a bigger τ (or longer MRR), the MRR's effect is more pronounced.

#221622 - $15.00 USD Received 25 Aug 2014; revised 18 Sep 2014; accepted 19 Sep 2014; published 23 Oct 2014

$$\frac{1}{v_{3dB}^2} \cong \frac{1}{v_{3dB,PD}^2} + \frac{1}{v_{3dB,MRR}^2} = \frac{1}{v_{3dB,PD}^2} + \frac{1}{(v/Q)^2} \tag{8}$$

3. Fabrication process

We use an 8-inch SOI wafer with a top Si thickness of 340 nm and a buried oxide (BOX) thickness of 2 µm. An oxide hard mask was used to etch the Si waveguides and MRR structures. A separate oxide hard mask was used for selective Ge epitaxy (see Fig. 3(a)). Before the Ge epitaxy, tetramethylammonium hydroxide (TMAH) at 50 °C for ~200 s was used to recess etch the silicon to improve Si waveguide to Ge coupling [15]. A remaining of ~200 nm silicon was left in the epitaxial window for Ge growth. Figure 3(b) shows the scanning electron microscope (SEM) image after TMAH etching. A 50 nm Ge/Si buffer layer and 500 nm pure Ge was grown by ultra-high vacuum chemical vapor deposition (UHV-CVD). Figure 3(c) shows the profile of germanium with a typical ~25° sidewall facet angle. In order to increase the coupling efficiency, we designed a 1 µm long Ge taper structure. With the ~25° germanium slope profile, this effectively becomes a 3-dimensional taper coupling the optical signal from the Si waveguide to Ge. After epitaxy, a partial etch to germanium was done to form a rib waveguide as shown in Fig. 3(d). Boron (p +) and Phosphorus (n +) implantation into Ge waveguide slab and side wall was done, followed by a 500 °C 30 s anneal to achieve a lateral electric field across the Ge waveguide, and for contact purposes. A lateral *pin* Ge diode was created across the Ge waveguide structure which is similar, but not identical to Ref [8]. Subsequently, a 150 nm thick TiN was deposited as the heater metal and 750 nm Al for metallization. Finally, a 400 nm SiO_2 was used for passivation. The optical image of the fabricated MRR enhanced photodetector is shown in Fig. 3(e) and Fig. 3(f). A high resolution transmission electron microscope (TEM) cross-section of fabricated device is shown in Fig. 3(g).

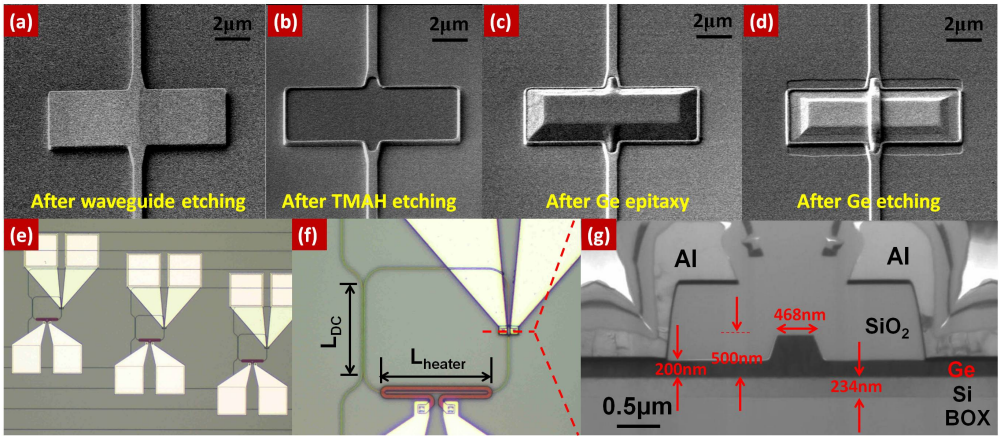

Fig. 3. SEM images (a) & (b) are before and after TMAH etch, (c) after Ge epitaxial, and (d) after Ge etching. (e) & (f) are optical microscope images of fabricated devices. (g) TEM cross-section image of fabricated device.

4. Characterization and discussion

4.1 Ultra-short PD

The PDs were first characterized on a conventional waveguide coupled configuration as shown in Fig. 1 (a). To extract the rib Ge waveguide propagation loss, PDs with six different lengths were used. The minimum device length was 4 µm, with a 2 µm increase for sequential length splits. The rib waveguide width was 600 nm, and the laser wavelength was 1600 nm with TE polarization. At −1 V reverse bias, output light power is shown in Fig. 4(a). From

#221622 - $15.00 USD Received 25 Aug 2014; revised 18 Sep 2014; accepted 19 Sep 2014; published 23 Oct 2014

linear fitting result, a rib Ge waveguide propagation loss of ~0.27 dB/μm was calculated. The device photocurrent and dark current are shown in Fig. 4(b). Under 1 V of forward and reverse bias, the currents are ~2.17 mA and ~7.89 nA, respectively. The excellent diode characteristics come from the good Ge epitaxial film quality, and optimization of the implant conditions. The ultra-low dark current was achievable due to the small device area and reduced lateral dopant diffusion with the short annealing time.

From the reference waveguide measurement results, we can estimate that the optical loss from tunable laser to Ge-PD is ~2.79 dB. Therefore, the input light power entering the PD is ~284 μW. Under this input power, the PD photocurrent is ~128 μA which gives a responsivity of ~0.45 A/W. The low responsivity was due to the short PD length where absorption is limited.

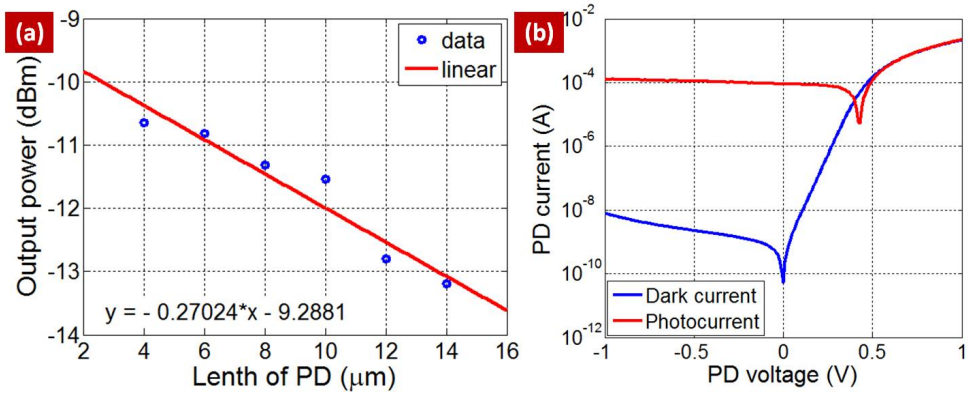

Fig. 4. (a) Propagation loss with different length PD. The reverse bias is −1 V, and laser wavelength is 1600 nm. (b) Photocurrent and dark current of a 4 μm PD.

4.2 MRR photodetector static characteristics

In this section, the 4 μm long Ge-PD was integrated in a MRR structure. The length of directional coupler was 60 μm, and gap was 300 nm. The bends had a radius of 10 μm. We use a tunable laser for TE-polarized scanning wavelengths in a range from 1595 nm to 1640 nm. The results are shown in Fig. 5(a). As comparision, a waveguide-coupled PD results is shown in green and superimposed on the plot, and red dotted line is the fitting result. A 2.0 times enhancement for the MRR PD was observed for resonant wavelengths. One of peak wavelength is zoomed in and fitted using a Lorentz function (see Fig. 5(b)). The full-width half maxmium (FWHM) is ~0.222 nm, leading to a Q value of ~7257 for the MRR. The relationship of Q and $t\gamma$ is obtained from Eq. (9). $t\gamma$ is calculated to be 0.735 given that the microring perimeter L is 282.8 μm and the optical group velocity n_g is ~4.3. Therefore, the maximum enhancement factor M_{os} is 2.15. So the responsivity will be increased from 0.45 A/W to 0.97 A/W.

$$Q = \frac{k_0 L n_g}{2} \frac{\sqrt{t\gamma}}{1 - t\gamma} \tag{9}$$

From Eq. (3), the coupling coefficient t is estimated to be ~0.92 and microring resonator γ is ~0.80. The mismatch in t and γ reduces the enhancement factor. This mismatch could possibly come from differences in design and fabricated dimensions. Heaters are widely used to tune MRR and directional coupler to improve the coupling factor [21,22].

For further discussion, a Ge detector as a ring was considered in our work. However, this provided a process challenge during the formation of Ge in a narrow epitaxial window of ~1 - 2 μm wide. In addition, the coupling efficiency between a Si waveguide and Ge ring was expected to be lower due to the faceted sidewalls of the Ge epitaxial film. Therefore, a Ge detector in a Si ring design as a MRR structure was adopted ultimately.

#221622 - $15.00 USD Received 25 Aug 2014; revised 18 Sep 2014; accepted 19 Sep 2014; published 23 Oct 2014

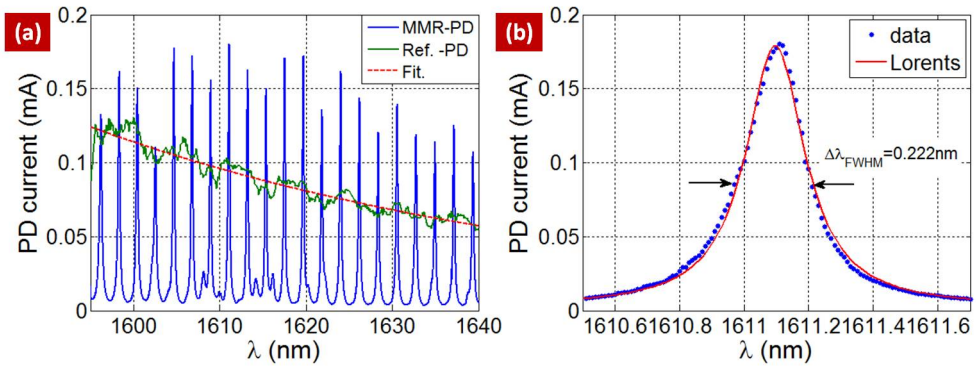

Fig. 5. (a) Photoresponse comparison between MRR enhanced PD (blue) and waveguide coupled PD (red). (b) Magnified image of a resonant peak. Center wavelength is 1611.1nm and bandwidth is 0.222 nm. Blue dots are measured data. Red line is Lorentz fitted results.

4.3 Frequency response and bandwidth

For *pin* waveguide PD, the 3-dB frequency response, $\upsilon_{3dB,PD}$ can be described by Eq. (10) [23]:

$$\frac{1}{\upsilon_{3dB,PD}^2} \cong \frac{1}{\upsilon_{3dB,RC}^2} + \frac{1}{\upsilon_{3dB,tr}^2} \tag{10}$$

Where $\upsilon_{3dB,RC}$ is the *RC*-limited bandwidth and $\upsilon_{3dB,tr}$ is the transit-time limited bandwidth.

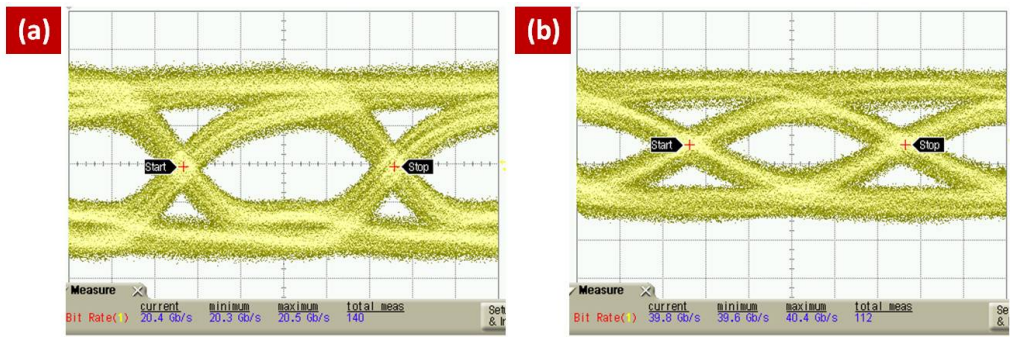

Fig. 6. (a). 20 Gb/s eye-diagram at –1 V reverse bias. (b) 40 Gb/s eye-diagram at –2 V reverse bias.

The MRR PD bandwidth is not limited by the theoretical Ge-PD bandwidth $\upsilon_{3dB,PD}$ given that the Ge-PD is very small. Instead, the limitation of device bandwidth is expected to come from the MRR structure. With a cycle time of 3.84 ps for the optical signal to complete a loop in the MRR, $\upsilon_{3dB,MRR}$ the upper limit of the device bandwidth is calculated to be ~25.7 GHz for this particular design. Nevertheless, high speed eye diagrams of 20 Gb/s and 40 Gb/s with reverse bias of –1 V and –2 V, respectively, are attained with the device. They are shown in Fig. 6(a) and 6(b).

4.4 Heater fine tuning and thermal characteristics

The integration of a heater is required for tuning to compensate for possible MRR oscillation wavelength mismatch. The heater covers part of the microring with a length of 100 μm and is 2 μm wide. The measured heater resistance was ~458 Ω. For measuring the heater tuning

#221622 - $15.00 USD Received 25 Aug 2014; revised 18 Sep 2014; accepted 19 Sep 2014; published 23 Oct 2014

capability, the input light wavelength was varied with different heater tuning voltage. When the input wavelength matches the MRR oscillation wavelength, maximum PD photocurrent response is obtained. This process illustrates a tracing function which is typically applied in label-free optical sensor applications [24–26]. Figure 7(a) further plots the PD photocurrent against heater power under different light wavelength. The wavelength of the input light is increased from 1603.5 nm to 1605.5 nm in steps of 0.5 nm. The heater powers corresponding to maximum PD photocurrent are shown in Fig. 7(b). The calculated slope is ~24 mW per nm. Given that the free spectral range (FSR) is ~2.16 nm, 51.7 mW of power will be required for a FSR shift. This heater efficiency can be improved by 20-folds by adopting an oxide undercut technology [25, 26].

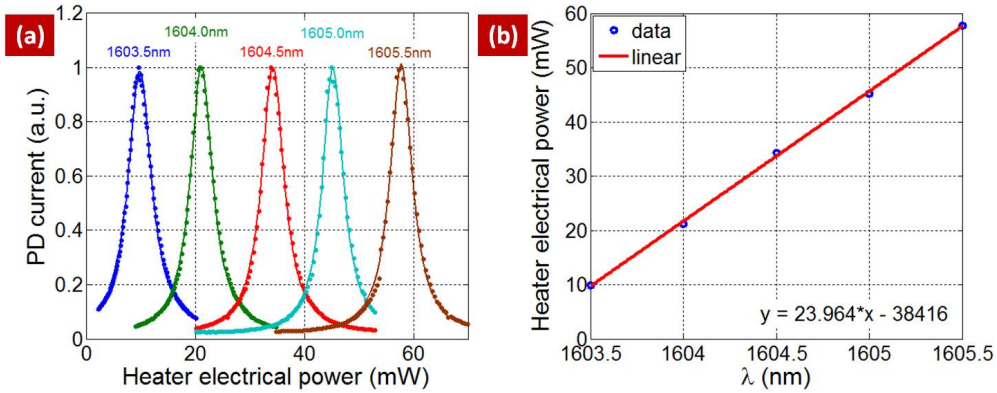

Fig. 7. (a) PD current vs. heater electrical power with different incident light wavelength. The wavelength is increasing from 1603.5 nm to 1605.5 nm by step of 0.5 nm. (b) The heater power curresponding to maximum photocurrent vs. incident wavelength.

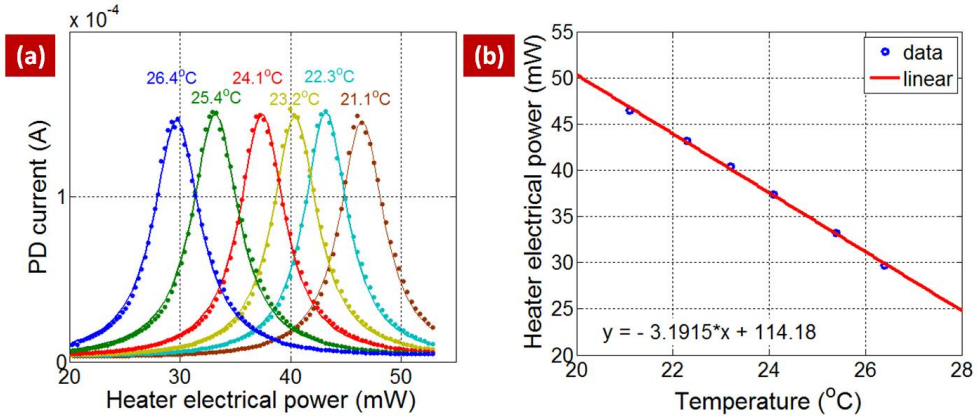

Fig. 8. (a) PD current vs. heater power for different temperature. (b) the peak heater power vs. temperature. The slope is ~3.2 mW/K.

The tracing function can be also by applied in temperature sensing application too. In this case, the oscillation wavelength's dependency on temperature is leveraged. In a practical application, the chip temperature can be controlled by electric temperature controller (ETC). Figure 8(a) shows the peak PD photocurrent under different heater power at varying temperatures. At higher temperatures, a lower heater power is required to achieve peak photocurrent. The relationship between heater powers corresponding to peak PD photocurrent current against chip temperature is shown in Fig. 8(b). The calculated sensitivity S is ~3.2 mW/K.

#221622 - $15.00 USD Received 25 Aug 2014; revised 18 Sep 2014; accepted 19 Sep 2014; published 23 Oct 2014

5. Conclusion

We proposed and demonstrated a mirocring resonator (MRR) enhanced photodetector (PD) structure. A very short PD of 4 μm in length was integrated in the MRR. The oscillation wavelength light was enhanced by the MRR and utilized to amplify the PD response. An enhancement factor of ~2 was achieved in PD responsvity at *L*-band wavelengths with 40 Gb/s capability demonstrated. Temperature sensitivity using a TiN heater for thermal tunability was investiaged as well. This device can be applied into WDM receiver systems.

Acknowledgments

This work was supported by the Science and Engineering Research Council of A*STAR (Agency for Science, Technology and Research), First author is also supported by National Natural Science Foundation of China (NSFC, Grant No. 61177090, 61377048).

#221622 - $15.00 USD Received 25 Aug 2014; revised 18 Sep 2014; accepted 19 Sep 2014; published 23 Oct 2014